Solid State Ionics 347 (2020) 115246

Contents lists available at ScienceDirect

Solid State Ionics

journal homepage: www.elsevier.com/locate/ssi

A novel single-ion conductor gel polymer electrolyte prepared by co-irradiation grafting and electrospinning process

Hang Li[a], Xiu Shen[b], Haiming Hua[b], Jingxiong Gao[b], Zhipeng Wen[b], Xin Wang[b], Longqing Peng[b], Dezhi Wu[c], Peng Zhang[a,*], Jinbao Zhao[a,b,*]

[a] College of Energy, Xiamen University, Xiamen 361005, PR China
[b] State Key Lab of Physical Chemistry of Solid Surfaces, Collaborative Innovation Centre of Chemistry for Energy Materials, Engineering Research Center of Electrochemical Technology, Ministry of Education, State-Province Joint Engineering Laboratory of Power Source Technology for New Energy Vehicle, College of Chemistry and Chemical Engineering, Xiamen University, Xiamen 361005, PR China
[c] School of Aerospace Engineering, Xiamen University, Xiamen 361005, China

ARTICLE INFO

Keywords:
Co-irradiation grafting
Single-ion conductor
PVDF-HFP backbone
Electrospinning

ABSTRACT

A novel way to manufacture single-ion conductor gel polymer electrolyte was reported in this work. Firstly, the γ-ray co-irradiation grafting is introduced to solve the difficulty on how to prepare single-ion conductor with considerable physical and chemical properties. Here, the PVDF-HFP is chosen as the polymer backbone for its excellent performance for polymer electrolyte while 2-acrylamido-2-methylpropanesulfonic acid (AMPS), a common and easily obtained double bond monomer with higher degree of negative charge delocalization, is chose to be the grafting monomer. To further promote the dissociation of Li^+ ions from the polyanions, the prepared grafting copolymer is spun into a nonwoven membrane with high porosity. Besides, the grafting copolymer nonwoven fabric transforms the crystal form of PVDF-HFP to a better β-phase with higher polarity and maintains an approximative thermal stability. After plasticized by EC/DMC solvent, this prepared single-ion conductor gel polymer electrolyte (SIC-GPE) presence a high lithium-ion transference number (LTN) of 0.97 with an outstanding electrochemical stability and an appropriate battery performance.

1. Introduction

Nowadays, the massive use of energy has raised severe energy shortages and environment pollutions. Solving the energy crisis is a gigantic systematic engineering process, while the traditional fossil energy should gradually be replaced by the green renewable energy. Developing an efficient large scale energy storage system plays an important role in building this advanced energy system [1,2]. Since commercialized in early 1990s, lithium-ion batteries (LIBs) have been concerned as the one of the best choice due to their high energy density, long cycle life and large output power [3,4]. However, the safety issue of LIBs has limited the further application mainly towing to the use of the liquid electrolyte which could cause leakage, side reaction and explosions [5,6]. As a result, solid electrolytes have been developed to eliminate the safety problems caused by liquid electrolytes.

In 1973, Wright et.al discovered that poly(ethylene oxide) (PEO) with alkali salts can lead ionic conduction. Then, Armand perceptively proposed the application of the Li-ion conducting systems as solid polymer electrolytes (SPEs) [7]. However, the conductivity of ordinary SPE at room temperature is normally only 10^{-6} S/cm [8,9], which could hardly apply in LIBs. In addition to lower ionic conductivity, polymer electrolytes also suffer a quite low lithium-ion transference number (LTN) which represents the ratio of conductivity contribution of lithium ion [10,11]. Since the lithium salt anions are non-electrochemical active, while the anions will accumulate on the surface of the electrode, causing concentration polarization which results in an increase in voltage losses and internal impedance as well as leading to the undesirable side reactions thus accelerating the deterioration of the cell. Furthermore, it has been calculated that an electrolyte with LTN approaching to 1 has a performance comparable to an dual-ion electrolyte even with a tenfold reduction in conductivity [12]. To this end, single-ion conductors (SICs), with LTN close to unity have attracted extensive attention and regarded as a promising way to overcome the drawbacks of SPEs. Among the main strategies to realize the single-ion conduction, attaching an anion onto the polymer matrix through a covalent bond should be the most effective routine to immobilize anions conduction with excellent electrochemical performance. However, there are two main challenges on preparing SICs by incorporating the

* Corresponding author.
E-mail address: jbzhao@xmu.edu.cn (J. Zhao).

https://doi.org/10.1016/j.ssi.2020.115246
Received 19 November 2019; Received in revised form 8 January 2020; Accepted 27 January 2020

anion as part of a polymer chain. One is to find a suitable lithium salt monomer with higher degree of negative charge delocalization to gain more free Li ions for conduction, while the other is to seek a proper way to link the corresponding salt monomer onto a stable backbone with higher mechanical and electrochemical stability. In recent, a lot of effort has been made on molecule design and synthesis of SICs [13–17]. A series of TFSILi-based lithium salt monomers were introduced to synthesis a SIC with high ionic conductivity since it shows strong electronic delocalization [18–21]. Armand et al. reported a "BAB" triblock single-ion solid polymer electrolyte based on lithium poly (styrene trifluoromethanesulphonylimide of lithium) P(SLiTFSI) and PEO with LTN around 0.85 and ionic conductivity of 1.3×10^{-5} S/cm at 60 °C [20]. Renaud Bouchet et al. compared a *block*-copolymer SIC with polystryrene-TFSI and polyacrylate-TFSI respectively [18]. Hansong Cheng et al. introduced bis(sulphonyl) imide lithium into a phenyl backbone to get a series of SICs [22,23]. Among strategies to attach the anions to polymer backbones, it is the mainstreaming practice to copolymerize a lithium salt monomer and an inert monomer providing mechanical strength or other specific function [24,25]. It brings researchers challenges to balance the ionic conductivity and physical properties like mechanical strength as they are strong dependent to the proportion of different monomers and the copolymerized structure.

Another feasible method is grafting lithium salt monomer directly onto a chosen polymer matrix with excellent physical properties. However, it is not easy to graft a monomer to a stable polymer matrix. The atom transfer radical polymerization (ATRP) is one of available method while it demands strict conditions for operation [26–28]. Irradiation grafting process which generates free radicals by high-energy ionizing radiation is another alternative way. Owing to ultra-high energy of ionizing radiation, the grafting process can be available with no harsh reaction conditions and no additional initiator or catalyst required. Comparing to ATRP, irradiation grafting is more convenient and controllable so that it has a potential for extensive industrial application.

In our present work, we grafted 2-acrylamido-2-methylpropane sulfonic acid (AMPS), a common double bond monomer with a lithiatable sulfonic acid group, onto a stable PVDF-HFP backbone by the co-irradiation grafting process of simply irradiating both monomer and polymer powder in one pot [29–32]. To enhance the PVDF-HFP matrix's plasticizing ability and promote the dissociation of Li^+ ions, a gel polymer electrolyte with high specific surface area is fabricated by electrospinning the grafted co-polymer. The obtained nonwoven fabric membrane with thin nanofiber structure presents ultra-high solvent uptake thus considerably improving lithium ion dissociation and conduction. The designed single-ion conductor gel polymer electrolyte (SIC-GPE) also exhibits wide electrochemical window, high LTN and remarkable cyclic performance. Furthermore, this is a meaningful exploration of a new approach to the preparation of single-ion conductors and related polymer electrolyte.

2. Experimental

2.1. Materials

2-Acrylamido-2-methylpropanesulfonic acid (AMPS) was purchased from Aladdin. Lithium hydroxide monohydrate ($LiOH{\cdot}H_2O$), mechanol (AR), *N*,*N*-dimethylformamide (DMF, AR) were purchased from Sinopharm Chemical Reagent Co., Ltd. PVDF-HFP with a HFP content of 12% was purchased from Jiejin Chemical Co., Ltd. All the other solvents and reagents were synthesis grade and used without purification.

2.2. Preparation of co-irradiation grafting copolymer

The PVDF-HFP powder was soaked in a solution of AMPS with a volume ratio of methanol: H_2O = 2:1, in which AMPS take a proportion of 40% in weight. CuSO4 at a concentration of 0.004 mol/L was added as a polymerization inhibitor to suppress the self-polymerization of AMPS. The sample was taking a co-irradiation grafting by ^{60}Co γ source at a total dose of 50 kGy under argon atmosphere. The AMPS grafted PVDF-HFP powder (AMPS-g-PH) was washed in a water-ethanol mixed solution (water:ethanol = 2:1 in vol.) then centrifuged and dried for 3 times to remove unreacted AMPS monomer and homopolymer.

2.3. Preparation of non-woven single-ion conductor membrane

AMPS-g-PH co-irradiation grafted polymer was lithiated by soaked in 1 mol/L LiOH solution for 24 h and remove the residual alkali by washing in deionized water for several times. The lithiated polymer (AMPSLi-g-PH) was dissolved in NMP to obtain a 14 wt% transparent solution. The solution was sonicated to eliminate the bubbles and then transfer to a syringe for electrospinning process. Non-woven single-ion conductor membrane was electrospun at a voltage of 15 kV and a bolus speed of 3.7 μL/min while the distance between roller collection and syringe is 24 cm. The non-wove single-ion conductor was then dried at 60 °C for 12 h for further to remove residual NMP. Besides, the PVDF-HFP powder was dissolved in NMP at 14 wt% and electrospun to PVDF-HFP non-woven membrane in the same way as a contrast sample for the following test.

2.4. Sample analysis

The structure of co-irradiation grafting copolymer sample was analyzed by NMR (Bruker AV400), FTIR (Nicolet iS5, Thermo Electron Co, USA) and XRD (Miniflex600, Rigaku Ltd.). The morphology of electrospinning membrane is observed by a cold-field emission electron microscope (s-4800, Hitachi) and the corresponding elemental mapping is obtained by the energy dispersive spectral (EDS) attaching. Thermogravimetric (TG) and differential scanning calorimeter (DSC) curves of electrospinning membrane were obtained by the synchronous thermal analyser (STA 449 F3/F5 Jupiter Netzsch) to characterize the thermal stability of the membrane. The solvent uptake test by measuring the weight of the membrane before and after soaking in EC/DMC (v:v = 1:1) solution and then calculate as follow [Eq. (1)]:

$$\text{Uptake} = \frac{W - W_0}{W_0} \tag{1}$$

where W_0 is the weight of membrane before soaking while W is that after soaking.

2.5. Electrochemical characterization

The non-woven single-ion conductor membrane was swollen by a solution of EC/DMC (v:v = 1:1) to obtain a single-ion conductor gel polymer electrolyte(SIC-GPE). The electrochemical stability window was displayed by a linear scanning voltammetry (LSV) test with a Li | SIC-GPE | SS (stainless steel) semi-blocking cell on an electrochemical workstation (CHI440B, Chenhua Co.). The test was carried out from 2 V to 6 V vs. Li^+/Li with a scanning rate of 1 mV/s. The lithium-ion transference number (LTN) was investigated on an Autolab electrochemical workstation. The measurement of LTN test is the steady-state current method in which the electrochemical impedance spectroscopy (EIS) was tested before and after the chronoamperometry [33]. The value of LTN was calculated by the equation as follow [Eq. (2)]:

$$\text{LTN} = \frac{I_s(V - I_0R_0)}{I_0(V - I_sR_s)} \tag{2}$$

In which R_0 and Rs represent the impedance before and after DC polarization while I_0 and Is represent initial and stable current during polarization. The ionic conductivity at the range of 30 °C to 80 °C was obtained by EIS on another electrochemical workstation (Solartron SI 1287). A LiFePO4-based cathode ($LiFePO_4$:PVDF binder:acetylene

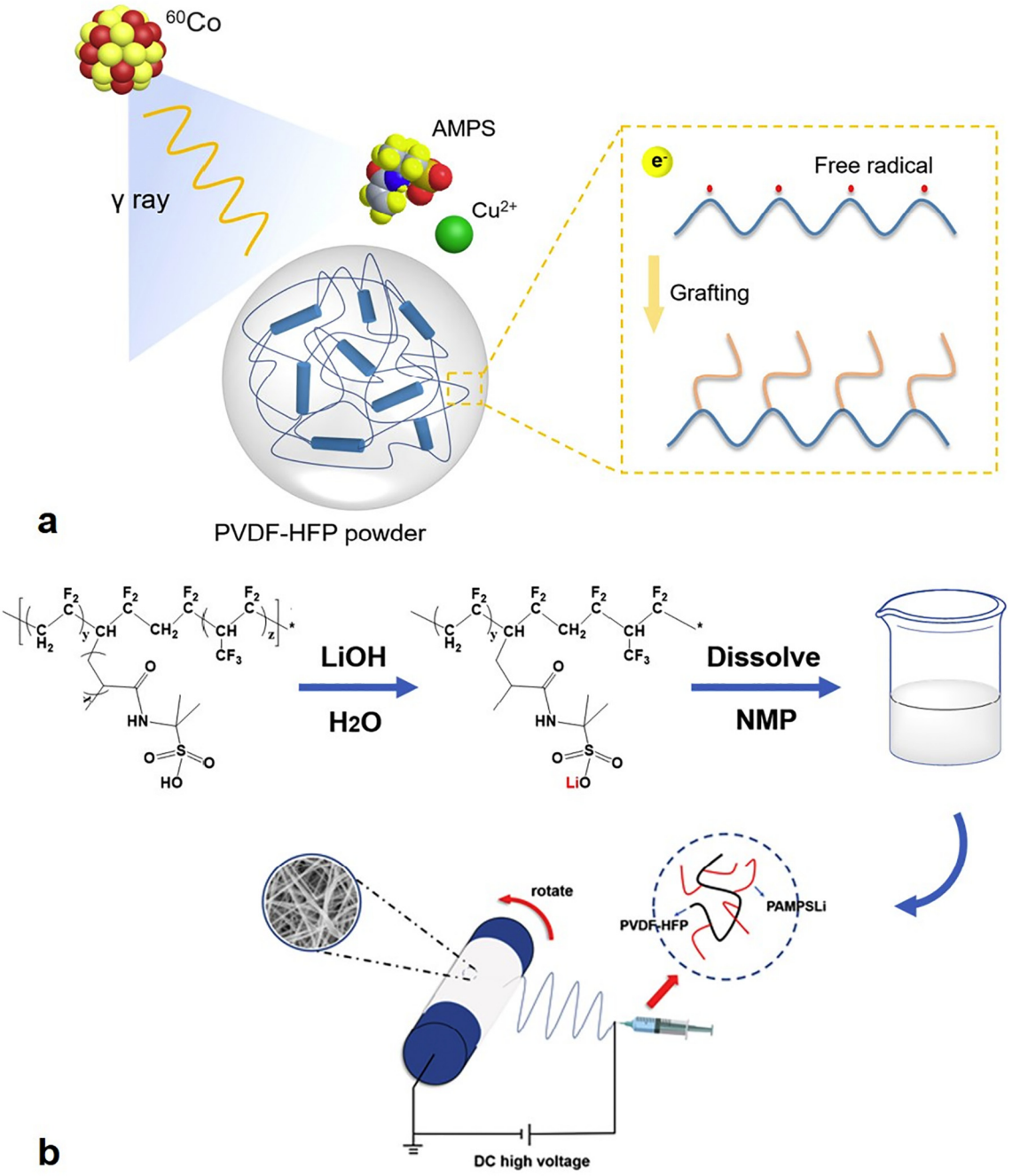

Scheme 1. (a) Mechanism of co-irradiation grafting process. (b) Preparation of electrospinning membrane from the lithiated co-irradiation grafting polymer.

black = 8:1:1 in weight) and a lithium metal anode were matched with the EC/DMC swollen SIC-GPE to assemble a type 2016 coin cell. The cycle and rate performances were investigated with those LFP half cells in a charge and discharge tester (Neware). all the cells mentioned were assembled in an argon glove box.

2.6. Computational information

The Molecular Dynamics (MD) Simulation and analysis were performed by GROMACS 2018software [34]. More details are shown in supporting information.

3. Results and discussion

The mechanism of heterogeneous co-irradiation grafting is demonstrated on Scheme 1(a). In this study, the PVDF-HFP powder was soaked in the AMPS monomer solution and was irradiated in argon atmosphere by γ ray at a dose of 50 kGy. Under the action of irradiation, the $–CH_2-$ or $–CF_2-$ group on PVDF-HFP chains generates free radicals and then initiates the grafting polymerization of AMPS monomer [35,36]. The adding of Cu^{2+} ion inhibitor was used to suppress the self-aggregation of AMPS by reducing free radicals generating in monomer solution, thus facilitate grafting process [37]. The co-irradiation grafting could happen in the amorphous region of the polymer matrix. And the prepared grafting co-polymer which has been lithiated was then dissolved and recrystallized during the electrospinning process. The spun grafted-polymer-salt PVDF-HFP would have a comb-like structure. In addition, the high porosity structure of non-woven fabric, together with the reduction of crystallinity, would provide an ultra-high liquid electrolyte uptake to form a gel polymer electrolyte which

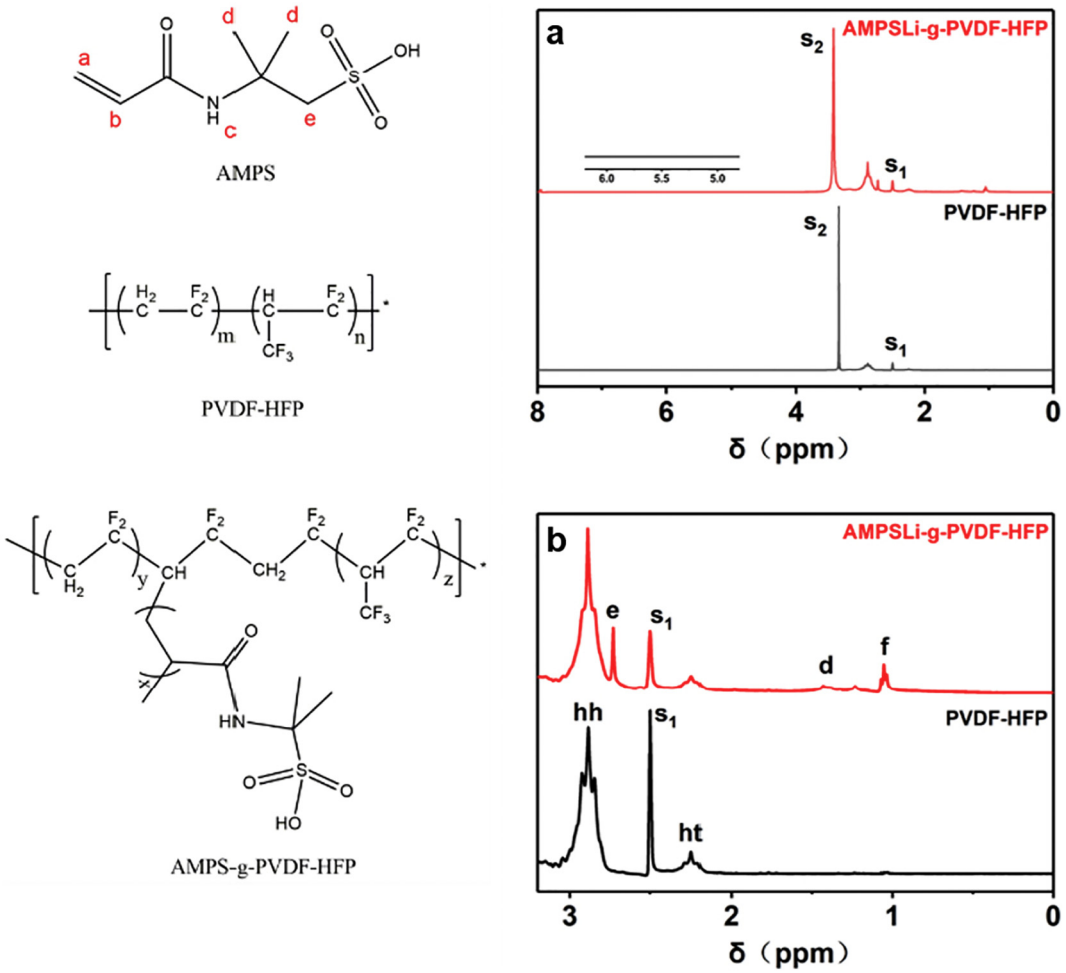

Fig. 1. The ^{1}H NMR spectra of washed AMPSLi-g-PVDF-HFP and PVDF-HFP, (a) a full view from 8 ppm to 0 ppm; (b) a partial view from 3.2 ppm to 0 ppm.

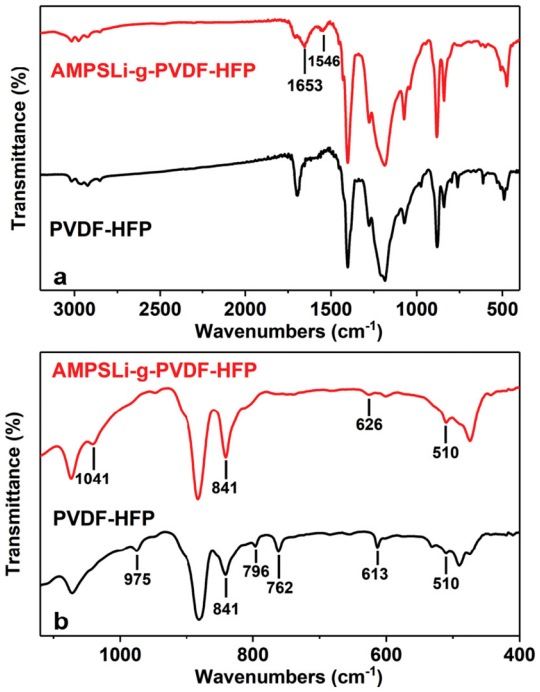

Fig. 2. The FTIR spectrum of AMPSLi-g-PVDF-HFP and PVDF-HFP of (a) a full view from 400 cm^{-1} to 3200 cm^{-1}; (b) a partial view from 400 cm^{-1} to 1120 cm^{-1}.

facilitates a higher ionic conductivity. The preparing of porous membrane process by electrospinning is illustrated on Scheme 1(b).

3.1. Characteristic of structure, morphology and physical properties

The structure of washed grafting polymer powder obtained from co-irradiation process is firstly verified by ^{1}H NMR spectra, as demonstrated on Fig. 1. The peaks S1 at δ = 2.5 ppm are attached to the solvent DMSO-d_6. The peak S2 belongs to water as an impurity peak. The slightly shifting of S2 to low field in grafting polymer's spectra is due to the presence of sulfonate group, which is hydrogen bonded with water molecules. No peak is observed at the region of 5–6 ppm, which indicates no AMPS monomer residues in the washed grafting copolymer retained since the δ = 5.50 ppm and δ = 6.03 ppm attributed to the H of CH_2 = CH– group in AMPS monomer as shown in Fig. S1. The peaks appear at δ = 1.4 ppm and δ = 2.7 ppm on washed *co*-irradiation grafting polymer's spectra represent protons labeled d and e, respectively. The peak at δ = 1.0 ppm matches the proton on hypomethyl, which is mainly contributed to the C=C double bonds in AMPS monomers taking a successful grafting polymerization reaction. The peaks at δ = 2.89 ppm and δ = 2.25 ppm are attributed to protons of methylene on the head-to-tail (ht) and head-to-head (hh) structure of PVDF-HFP backbone [38,39]. As a result, it would be reasonable to infer from the analysis above that the co-irradiation grafting polymerization was successful and the AMPS monomer was removed completely. It could be also estimated from the NMR spectrum analysis a structure of the obtained grafting co-polymer in which the polymerized AMPS branch is anchored in the PVDF-HFP matrix. The co-irradiation

grafting polymer is herein after referred to as AMPSLi-g-PVDF-HFP.

The FTIR spectrum of AMPSLi-g-PVDF-HFP non-woven membrane was displayed in Fig. 2 as well as the pure PVDF-HFP. The peak at 1653 cm^{-1} refer to stretching vibration of carbonyl group on secondary amide and the peak at 1546 cm^{-1} correspond to –CNH in-plane angular vibration, which is known as amide II absorption band [40–42]. These two characteristic peaks indicated AMPS monomer was grafted onto the matrix of PVDF-HFP. Compared with spectra of AMPS monomer (Fig. S2), the absence of C=C absorption peak at 1613 cm^{-1} infer the AMPS monomer was removed from the grafting polymer after washing by water-ethanol mixed solution. This result is consistent well with that of NMR analysis. In the partially amplified IR spectrum (Fig. 2(b)), two slightly absorption peaks at 1041 cm^{-1} and 626 cm^{-1} refer to symmetrical stretching vibration and in-plane bending vibration of sulfonic acid group respectively [43]. Together with the NMR analysis, those IR absorption peaks attached to AMPS-based grafting polymer imply a successful co-irradiation grafting again. What's more, the result of FTIR also reveals a crystal transformation of PVDF-HFP from a non-polar α-phase to a polar β-phase. As is illustrated in partially amplified IR spectrum, in the spectra of AMPSLi-g-PVDF-HFP, the absorption peaks at 975, 796, 762 and 612 cm^{-1} which correspond to the α-phase of PVDF-HFP disappear while a β-phase peak at 474 cm^{-1} emerges and the peak refer to β-phases at 841 cm^{-1} and 510 cm^{-1} strength in relative intensity [44,45]. It could be concluded that the grafting of polymer salt changes the crystal form of PVDF-HFP from a nonpolar phase with low dielectric constant to a polar phase with a higher dielectric constant. It is known that the dissociation of Li^+ with anion in the SICs is critical to gain much more free Li^+ for the ionic conductance. While this higher dielectric constant phase of polymer matrix could promote the dissociation of Li^+, herein improve the density of free carrier in the polymer electrolyte and increase the ionic conductivity.

The phase transition of the AMPSLi-g-PVDF-HFP could also be confirmed by the XRD pattern shown in Fig. 3. It vanishes in the AMPSLi-g-PVDF-HFP XRD pattern the peaks indicating a presence of α phase at $2\theta = 18.2^\circ$ and 19.9° which refer to the diffraction in planes (020) and (110) respectively. Relatively, a peak at $2\theta = 20.6^\circ$ clearly appears, referent to a superposition of (110) and (200) crystal plane diffraction. This peak represents the presence of both α phase and β phase as (110) plane refers to α phase while (200) plane correspond to β phase [46,47]. The results of XRD further reveal a transition from a non-polar phase to a polar one would happen when grafting a polymer salt to PVDF-HFP matrix. What's more, the XRD pattern shows a slightly decrease of crystallinity after grafting process. It could also be attributed to the introducing of polymer salt by breaking the regularity of backbone.

The morphology of electrospinning membrane is shown in Fig. 4. The non-woven AMPSLi-g-PVDF-HFP membrane is white in colour with flexible form as is shown in Fig. 4(a). The micro-structure of membrane is revealed by SEM. Fig. 4(b) and (c) show that the membrane is formed by polymer fibers. The diameter distribution of fibers was counted as shown in Fig. 4(d). Most of the fibers have the diameter of 300 nm–400 nm, the distribution of fibers conforms to the normal distribution. The super fine fiber structure with high porosity leads to an ultrahigh liquid uptake, which is up to 439%. It reveals that our strategy of promoting plasticizing ability of co-polymer to enlarge the interaction between polymer matrix and liquid solvent by electrospinning method is effective. The element mapping images of feature elements is obtained by the element dispersive spectral (EDS) and displayed in Fig. 5, in where F element is attached to PVDF-HFP matrix and S elements are subordinated to AMPSLi grafted polymer salt. It can be also observed from the mapping of non-woven single-ion conductor that the S element was existence and evenly distributed. In the other word, the polymer salt, grafted AMPSLi co-polymer, has a uniform distribution, which would result in a uniform current density when it is used as an electrolyte.

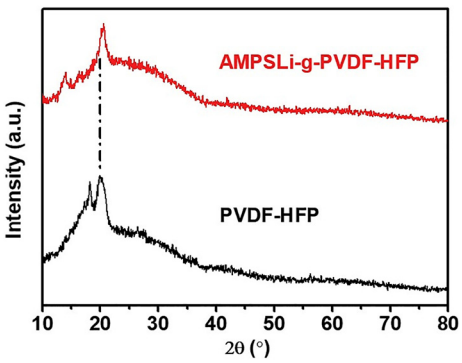

Fig. 3. The XRD pattern of AMPSLi-g-PVDF-HFP and PVDF-HFP.

The thermal stability of co-irradiation grafting polymer is not deteriorated as we can infer from the TG curves as shown in Fig. 6. There is no big difference between the decomposition temperature of PVDF-HFP and AMPSLi-g-PVDF-HFP non-woven membrane. PVDF-HFP decomposed at ca. 451.5 °C to 473.5 °C whereas AMPSLi-g-PVDF-HFP decomposed at the range of ca. 453.4 °C–476.3 °C. The differential scanning calorimeter (DSC) analysis in Fig. 6(b) displays two broad peaks of AMPSLi-g-PVDF-HFP and PVDF-HFP. The melting temperature of AMPSLi-g-PVDF-HFP is close to PVDF-HFP at ca. 137 °C. It could be integrated the melting enthalpy of AMPSLi-g-PVDF-HFP is 27.85 J/g while the contrast PVDF-HFP's is 35.04 J/g. The crystallinity can be counted by the following equation [Eq. (3)]:

$$X_c = \frac{\Delta H_f}{\Delta H_{100}} \times 100\% \quad (3)$$

where ΔH_f is the melting enthalpy of the sample and ΔH_{100} represents the standard melting enthalpy which is the enthalpy of fusion of 100% crystalline polymer. The crystallinity of PVDF-HFP is 33.5% whereas AMPSLi-g-PVDF-HFP's is 26.6%. The slightly decrease of crystallinity is owing to the grafting copolymer with comb-like structure break the regularity of PVDF-HFP segment during the recrystallization. It can be concluded that the thermal stability of grafting co-polymer is enough for applying in LIBs. In addition, a decrease in crystallinity aid to increase the plasticizer uptake, hence elevating the ionic conductivity.

3.2. Electrochemical performance

The prepared non-woven AMPSLi-g-PVDF-HFP membrane is plasticized by EC/DMC (1:1 in vol.) to form a gel polymer electrolyte named SIC-GPE. The electrochemical stability is firstly characterized by linear sweep voltammetry as shown in Fig. 7(a). A Li|SIC-GPE|SS 2016 type cell in which stainless steel is an inactive electrode and Li foil is the counter and reference electrode are used while the sweep rate of 1 mV/s is adopted over a wide potential range between 2 V and 6 V. As indicated by the red dash line, the decomposition current with a density higher than 10 $\mu A/cm^2$ is detected at 4.8 V vs. Li^+/Li. Then, the current rises sharply after 4.9 V, indicating a severe oxidation of SIC-GPE. The result shows a wide electrochemical window of SIC-GPE, which is much wider than most of commercial electrolytes with polyolefin separators. Such a wide electrochemical window exceeding 4.8 V ensures most common cathode materials can match with SIC-GPE without having to worry about the oxidative decomposition of electrolyte. The excellent electrochemical stability of PVDF-HFP matrix determines the stability of SIC-GPE, hence achieving a wide electrochemical window for practical application. The remarkable electrochemical elevates the safety of electrolyte and shows application potential in high-voltage lithium batteries.

The lithium-ion transference number (LTN) is investigated by the steady current method and the result is demonstrated in Fig. 7(b). It can be calculated that the interface impedances before and after the

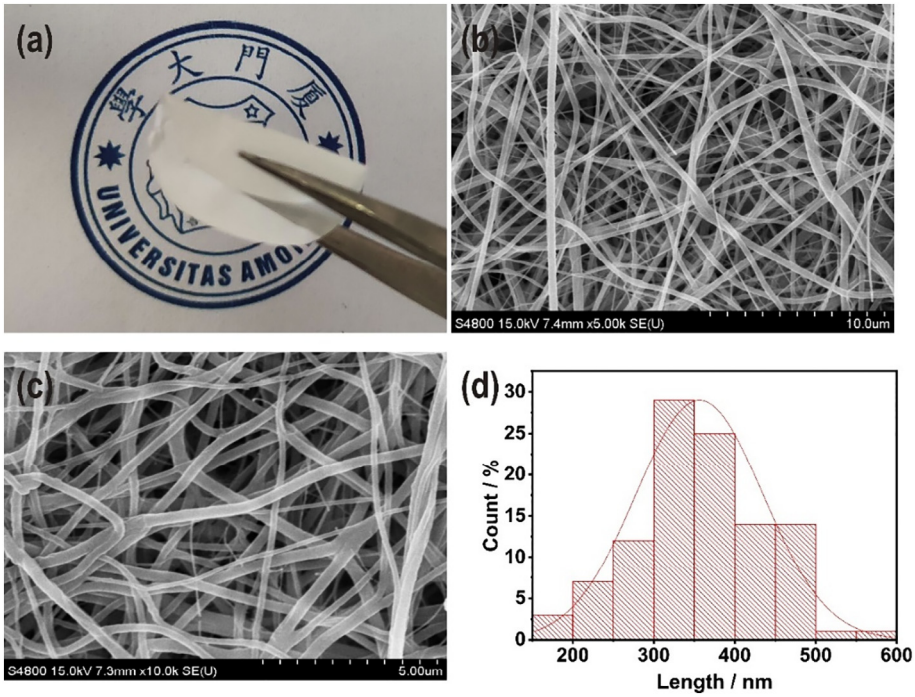

Fig. 4. (a) The optical image of prepared single-ion conductor non-woven; (b), (c) corresponding surface SEM images with different magnifications of ×5000, ×10,000 respectively; (d) the diameter length distribution of single-ion conductor non-woven fabric.

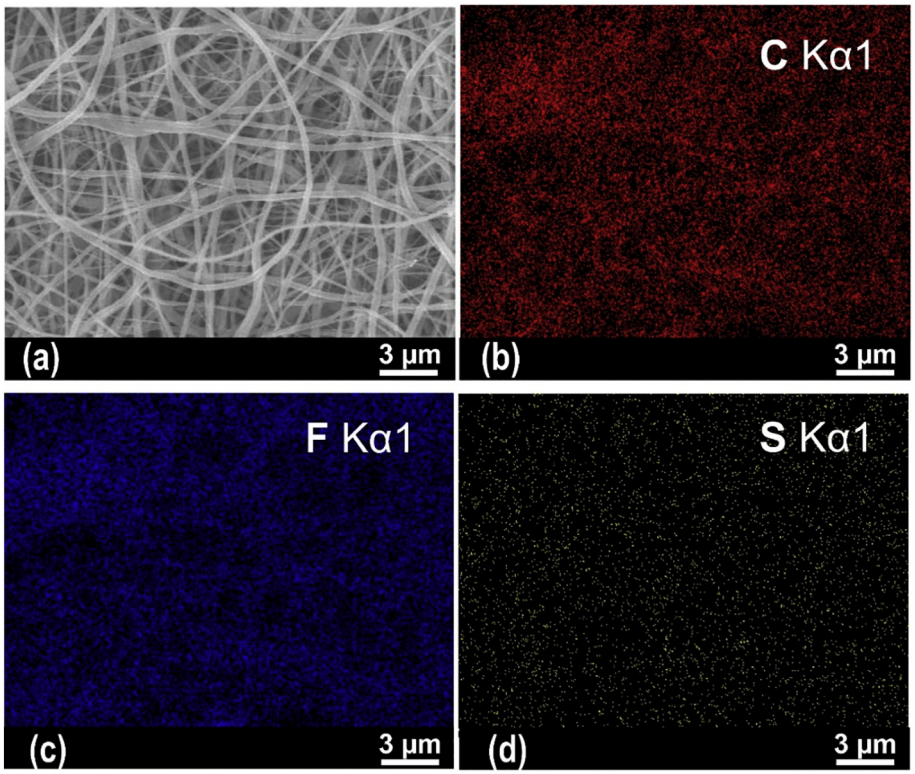

Fig. 5. Element dispersive spectral (EDS) results, (a) corresponding SEM image, (b)–(d) shows elements mapping of C, F, and S respectively.

chronoamperometry are 1900 Ω and 2065 Ω, respectively. The initial current at a polarization voltage of 10 mV is detected 14.3 μA whereas the stable-state current valued 13.2 μA. Based on the equation of lithium-ion transference number involved in experiment section [Eq. (4)], the calculated LTN is 0.97, close to unity. The high LTN value illustrates the single-ion transporting characteristic of our prepared SIC-GPE. That is, the anions are anchored in the matrix of grafting co-polymer by covalent bond while the Li^+ are dissociated in the high dielectric solvent of EC/DMC, what's more, the polar β-phase of PVDF-HFP obtained from the grafting co-polymer process also facilitate to the dissociation of polymer salts. A high LTN means low concentration polarization would be caused as little anion accumulated on the

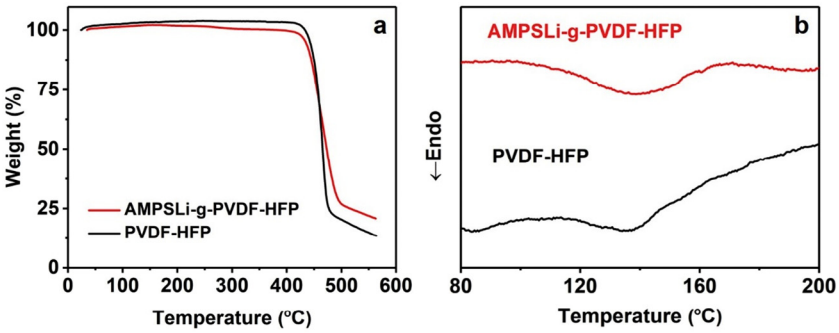

Fig. 6. (a) TG curves and (b) DSC curves of AMPSLi-g-PVDF-HFP and PVDF-HFP membrane.

electrode surface which could induce undesirable reaction. Furthermore, a high LTN also exhibit a much higher lithium ion conductivity compared with those electrolytes who have the same conductivity since the LTN of ordinary polymer electrolyte is usually less than 0.5 due to a slower transference of lithium ions compared with counter anions. It was reported that a single-ion electrolyte with a LTN equal to 1 has a comparable performance as a dual-ion one having a conductivity ten-fold higher [12]. Since the inactive counter anions are blocking to the electrode, the lithium ion conductivity, which equals to a product of total ionic conductivity and LTN, is the effective conductivity for electrolyte. Thus, a close-to-unity LTN of SIC-GPE means the elimination of concentration polarization and the elevation of effective ionic conductivity.

The ionic conductivities of SIC-GPE at different temperatures are then displayed in Fig. 7(c). The conductivity of SIC-GPE is 3.4×10^{-5} S/cm at 30 °C and 7.8×10^{-5} S/cm at 60 °C. As is shown in Fig. 7(d), the relationship between ionic conductivity and temperature is in accordance with Arrhenius equation [Eq. (4)]:

$$\sigma = \sigma_0 e^{\frac{-E_a}{RT}} \quad (4)$$

In the equation, the pre-exponential factor σ_0 represents the conductivity when the temperature is infinity while E_a is the apparent activation energy of ionic conduction. R and T represent ideal gas constant and temperature, respectively. It can be calculated the E_a of lithium ionic transportation is 6.18 kJ/mol. The ionic conductivity of the SIC-GPE is not very high. However, the LTN close to 1 make it a relatively high lithium ion conductivity comparable to the ordinary dual ion conducting GPE has a LTN at only 0.2–0.4 [11,48–50].

3.3. Battery performance

The cycling performance of LFP|SIC-GPE|Li cell is illustrated in Fig. 8(a). The test was carried out at 25 °C in a current rate of 0.2 C. After the first several cycles of activation process, the capacity was slowly increased and then stabilized at around 156 mAh/g. The coulombic efficiency was maintained at a range of 99% to 100%. The discharge capacity of 100th cycle is 152.8 mAh/g and the corresponding coulombic efficiency is 99.7%. Although the SIC-GPE does not demonstrate a high ionic conductivity, the single-ion conducting characteristic promotes to achieve a stable cycling performance with high coulombic efficiency. In the other word, the elimination of concentration polarization and relatively high lithium ion conductivity facilitate an acceptable cycling performance. The rate performance is demonstrated in Fig. 8(b). The discharge capacities of 0.1 C and 0.2 C are close, at ca. 150 mAh/g. The discharge capacity then dropped to around 129 mAh/g at 0.5 C. And the discharge capacity remains about 100 mAh/g as the rate is further increased to 1 C. Finally, the discharge capacity is stabled at around 150 mAh/g when the rate is falling back to 0.1 C. It is still relatively good performance considering the total ionic conductivity of SIC-GPE is one tenth of a commercial electrolyte-

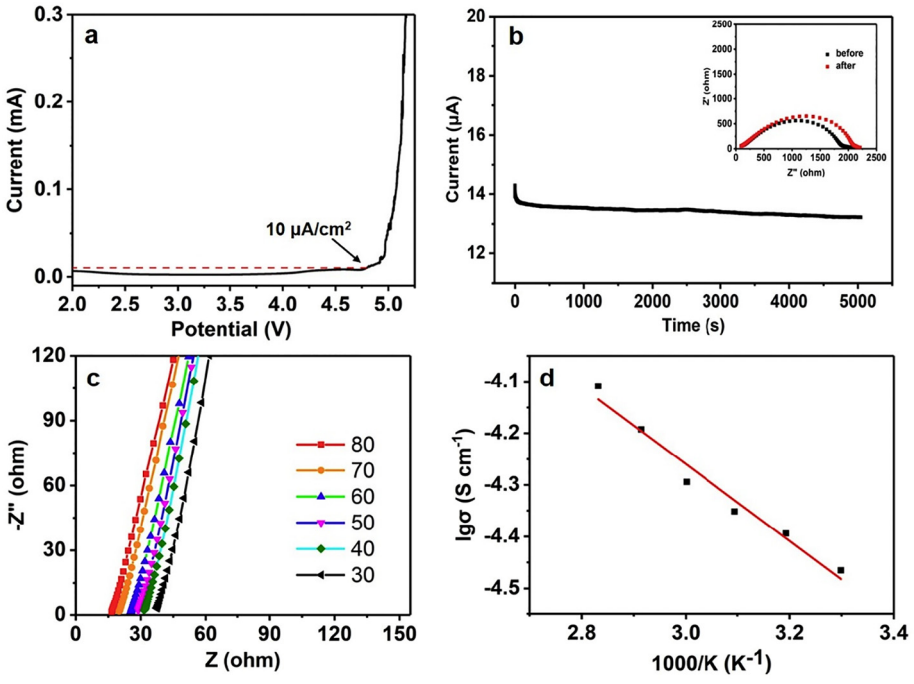

Fig. 7. (a) The LSV curves of Li|SIC-GPE|SS asymmetrical cell with a sweep rate of 1 mV/s; (b) the i-t curves of chronoamperometry of the Li|SIC-GPE|Li symmetrical cell with an insert image corresponding to EIS plots before and after chronoamperometry; (c) ionic conductivities of SIC-GPE at different temperatures; (d) Arrhenius behavior of SIC-GPE.

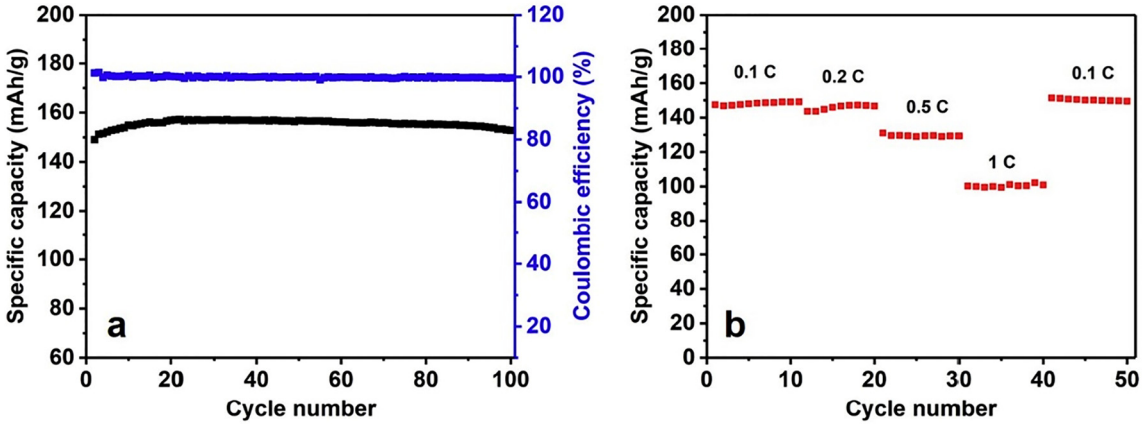

Fig. 8. (a) Cycle performance of LFP|SIC-GPE|Li coin cell at 25 °C, 0.2C; (b) rate performance of LFP|SIC-GPE|Licoin cell at 25 °C.

separator system. That is, the ultra-high LTN make up for the low apparent ionic conductivity and reduce the polarization, hence improve the rate performance.

3.4. Molecular dynamics simulation

To further understand the migration mechanism of lithium ions in a single-ion conductor gel polymer electrolyte and the relationship between the ionic conductivity and the amount of adding plasticizer, molecular dynamics simulation of systems with different solvent/polymer mass rate (0:1, 1:8, 1:4, 1:2 and 1:1) have been done. The radial distribution function and the coordination number integrated from it of Li^+ before (mass rate = 0:1) and after plasticizing (mass rate = 1:1) was shown in Fig. 9. The coordination number at 2.3 Å of all systems was listed in Table 1. Before plasticizing, the coordination number with O atoms of sulfonate reaches 2.81 (Table 1). The high coordination number indicates a tightly binding of sulfonate and Li^+. After adding EC/DMC plasticizer, the coordination number of lithium to sulfonate oxygen reduced to 2.18 while that to carbonyl oxygen atoms of EC/DMC increased to 1.61 gradually, which shows Li cations are more easily to ionize. In other word, the high-dielectric-constant EC/DMC plasticizer could facilitate the dissociation of Li^+ by coordinate with it, thus promote the migration of Li^+.

The mean square displacement (MSD) function in Fig. 10 indicates that the diffusion coefficient of Li ions (D_{Li}) is greatly increased after the addition of the plasticizer. Table 2 shows the values of D_{Li} corresponding to different solvent/polymer mass rate calculated from MSD function in Fig. 10. With an elevation of solvent/polymer mass rate from 0:1 to 1:1, we can see a great improve of D_{Li} from

Table 1
Coordination number of Li + with different groups of different solvent/polymer mass rate.

Solvent/polymer mass rate	0: 1	1: 8	1: 4	1: 2	1: 1
O ($-SO^{3-}$)	2.81	2.50	2.40	2.29	2.18
C═O (polymer)	0.63	0.49	0.45	0.32	0.30
F (polymer)	0.37	0.14	0.24	0.00	0.00
C═O (EC)	–	0.47	0.66	0.66	0.94
C═O (DMC)	–	0.35	0.46	0.78	0.67

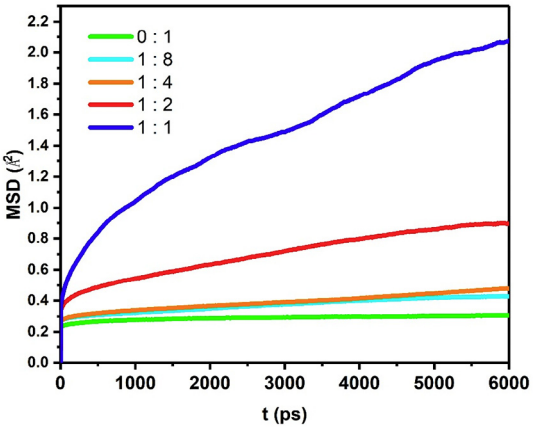

Fig. 10. MSD curves of different solvent/polymer mass ratio.

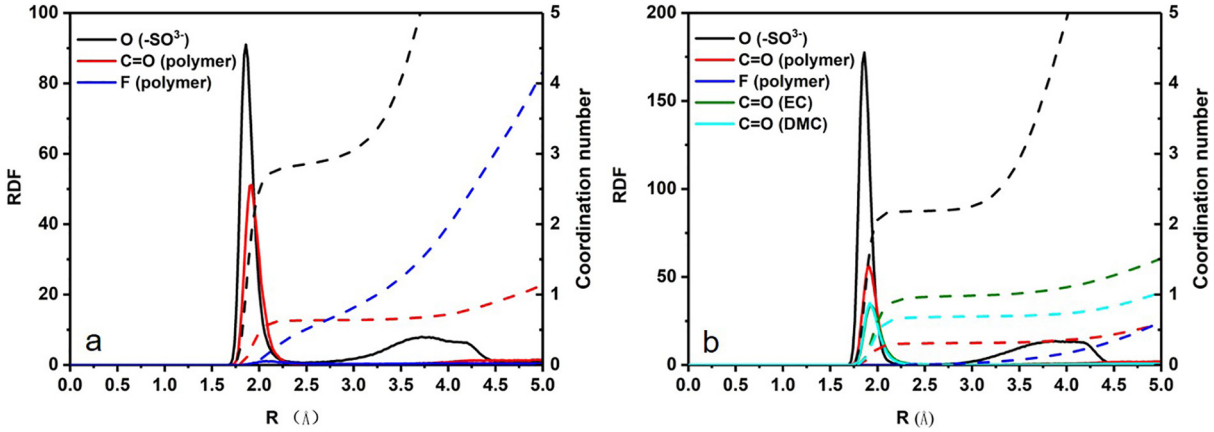

Fig. 9. (a) The radial distribution function (RDF) (solid line) and the coordination number (dashed line) before plasticizing; (b) the radial distribution function (RDF) (solid line) and the coordination number (dashed line) of mixture whose mass rate of solvent/polymer is 1:1.

Table 2
The diffusion coefficient of Li^+ with different groups of different solvent/polymer mass rate.

Solvent/polymer mass rate	0:1	1:8	1:4	1:2	1:1
D_{Li} ($\times 10^{-10}$ cm^2/s)	3.71	5.19	5.86	7.56	21.3

3.71×10^{-10} cm^2/s to 2.13×10^{-9} cm^2/s. It can descript qualitatively that the Li cation mobility is greatly improved. The increased mobility of Li cation is probably caused by an increase in ionic dissociation and a decrease in viscosity after adding plasticizer. It could be concluded that the computation results support the strategy of electrospinning the co-irradiation grafting polymer, by which could greatly improve the plasticizer uptake as well as enlarge the contract surface area between the single-ion conductor and the liquid solvent, consequently improving the ionic conductivity.

4. Conclusion

To obtain a single-ion conductor with stable physical and chemical properties, a co-irradiation grafting method was adopted to graft single-ion monomers to the stable PVDF-HFP chains, which is difficult to realize in conventional approaches. The co-irradiation grafting is confirmed successful and the prepared co-polymer shows thermal stability approaching to pure PVDF-HFP. It is worth noting that the grafted polymer salt transforms the crystal form of PVDF-HFP matrix to a high dielectric constant polar phase which would promote lithium salt dissociation. Electrospinning technique was introduced to enhance the PVDF-HFP matrix's plasticizing ability. The electrospinning single-ion non-woven fabric shows a high porosity and a uniform distribution of lithium salt at the nanoscale, inferring a high plasticizer uptake and evenly carrier distribution. Owing to the high electrochemical stability of PVDF-HFP matrix, the prepared SIC-GPE has a wide electrochemical window. The lithium-ion transference is close to unity at 0.97, showing single-ion conducting characteristic. The ionic conductivity at 30 °C is 3.4×10^{-5} S/cm. the assembled Li-$LiFePO_4$ coin cell with SIC-GPE shows a stable cycle performance and appropriate rate performance due to its high LTN. It is indicated that the co-irradiation grafted SIC-GPE has a considerable comprehensive performance. As a convenience way to graft specific monomers to a stable matrix, which is difficult by common method, co-irradiation graft has a broad application prospects on fabricating single-ion conductors of a particular design.

CRediT authorship contribution statement

Hang Li: Methodology, Validation, Writing - original draft. **Xiu Shen:** Validation, Formal analysis. **Haiming Hua:** Software. **Jingxiong Gao:** Validation. **Zhipeng Wen:** Validation. **Xin Wang:** Formal analysis. **Longqing Peng:** Validation. **Dezhi Wu:** Resources. **Peng Zhang:** Conceptualization, Writing - review & editing. **Jinbao Zhao:** Supervision, Resources.

Declaration of competing interest

The authors declare that they have no known competing financial interests or personal relationships that could have appeared to influence the work reported in this paper.

Acknowledgements

The authors gratefully acknowledge financial support from the National Natural Science Foundation of China [Grant numbers 21875195, 21503180, 21621091], the Fundamental Research Funds for the Central Universities [Grant number 20720170037] and the National Key Research and Development Program of China [Grant number 2017YFB0102000].

Appendix A. Supplementary data

Supplementary data to this article can be found online at https://doi.org/10.1016/j.ssi.2020.115246.

References

[1] M.M. Thackeray, C. Wolverton, E.D. Isaacs, Energy Environ. Sci. 5 (7) (2012) 7854.
[2] B. Dunn, H. Kamath, J.M. Tarascon, Science 334 (6058) (2011) 928.
[3] J. Tollefson, Nature 456 (7221) (2008) 436.
[4] X. Cheng, J. Pan, Y. Zhao, M. Liao, H. Peng, Adv. Energy Mater. 8 (7) (2018).
[5] J. Hassoun, B. Scrosati, J. Electrochem. Soc. 162 (14) (2015) A2582.
[6] L. Peng, X. Shen, J. Dai, X. Wang, J. Zeng, B. Huang, H. Li, P. Zhang, J. Zhao, J. Electrochem. Soc. 166 (10) (2019) A2111.
[7] D.E. Fenton, J.M. Parker, P.V. Wright, Polymer 14 (11) (1973) 589.
[8] L. Lu, X. Han, J. Li, J. Hua, M. Ouyang, J. Power Sources 226 (2013) 272.
[9] D. He, D.W. Kim, J.S. Park, S.Y. Cho, Y. Kang, J. Power Sources 244 (2013) 170.
[10] E. Quartarone, P. Mustarelli, Chem. Soc. Rev. 40 (5) (2011) 2525.
[11] V. Di Noto, S. Lavina, G.A. Giffin, E. Negro, B. Scrosati, Electrochim. Acta 57 (2011) 4.
[12] M. Doyle, T.F. Fuller, J. Newman, Electrochim. Acta 39 (13) (1994) 2073.
[13] H. Zhang, F. Lian, L. Bai, N. Meng, C. Xu, J. Membr. Sci. 552 (2018) 349.
[14] F. Lian, H.-y. Guan, Y. Wen, X.-r. Pan, J. Membr. Sci. 469 (2014) 67.
[15] P.-Y. Ji, J. Fang, Y.-Y. Zhang, P. Zhang, J.-B. Zhao, ChemElectroChem 4 (9) (2017) 2352.
[16] Q. Ma, H. Zhang, C. Zhou, L. Zheng, P. Cheng, J. Nie, W. Feng, Y.-S. Hu, H. Li, X. Huang, L. Chen, M. Armand, Z. Zhou, Angew. Chem. Int. Ed. 55 (7) (2016) 2521.
[17] E. Strauss, S. Menkin, D. Golodnitsky, J. Solid State Electrochem. 21 (7) (2017) 1879.
[18] D. Devaux, L. Liénafa, E. Beaudoin, S. Maria, T.N.T. Phan, D. Gigmes, E. Giroud, P. Davidson, R. Bouchet, Electrochim. Acta 269 (2018).
[19] S. Feng, D. Shi, F. Liu, L. Zheng, J. Nie, W. Feng, X. Huang, M. Armand, Z. Zhou, Electrochim. Acta 93 (2013) 254.
[20] B. Renaud, M. Sébastien, M. Rachid, A. Abdelmaula, L. Livie, B. Jean-Pierre, T.N.T. Phan, B. Denis, G. Didier, D. Didier, Nat. Mater. 12 (5) (2013) 452.
[21] L. Porcarelli, A.S. Shaplov, M. Salsamendi, J.R. Nair, Y.S. Vygodskii, D. Mecerreyes, C. Gerbaldi, ACS Appl. Mater. Interfaces 8 (16) (2016) 10350.
[22] Y. Chen, Y. Tian, Z. Li, N. Zhang, D. Zeng, G. Xu, Y. Zhang, Y. Sun, H. Ke, H. Cheng, J. Membr. Sci. 566 (2018) 181.
[23] C. Li, B. Qin, Y. Zhang, A. Varzi, S. Passerini, J. Wang, J. Dong, D. Zeng, Z. Liu, H. Cheng, Adv. Energy Mater. 9 (10) (2019).
[24] X. Shen, L. Peng, R. Li, H. Li, X. Wang, B. Huang, D. Wu, P. Zhang, J. Zhao, ChemElectroChem 6 (17) (2019) 4483.
[25] X.-G. Sun, J. Hou, J.B. Kerr, Electrochim. Acta 50 (5) (2005) 1139.
[26] K. Matyjaszewski, Macromolecules 45 (10) (2012) 4015.
[27] Y. Sui, Z.N. Wang, X.L. Gao, C.J. Gao, J. Membr. Sci. 413 (2012) 38.
[28] C. Perruchot, M.A. Khan, A. Kamitsi, S.P. Armes, T. von Werne, T.E. Patten, Langmuir 17 (15) (2001) 4479.
[29] Y. Zhu, F. Wang, L. Liu, S. Xiao, Z. Chang, Y. Wu, Energy Environ. Sci. 6 (2) (2013) 618.
[30] J. Hassoun, S. Panero, P. Reale, B. Scrosati, Adv. Mater. 21 (47) (2009) 4807.
[31] A.A. Conte, K. Shirvani, H. Hones, A. Wildgoose, Y. Xue, R. Najjar, X. Hu, W. Xue, V.Z. Beachley, Polymer 171 (2019) 192.
[32] H. Zhang, Y. Zhang, Z. Yao, A.E. John, Y. Li, W. Li, B. Zhu, Electrochim. Acta 204 (2016) 176.
[33] J. Evans, C.A. Vincent, P.G. Bruce, Polymer 28 (13) (1987) 2324.
[34] M.J. Abraham, T. Murtola, R. Schulz, S. Páll, J.C. Smith, B. Hess, E. Lindahl, SoftwareX 1-2 (2015) 19.
[35] J.N. Helbert, B.E. Wagner, E.H. Poindexter, L. Kevan, J. Polym. Sci. Polym. Phys. Ed. 13 (4) (1975) 825.
[36] M.C. Clochard, J. Bègue, A. Lafon, D. Caldemaison, C. Bittencourt, J.J. Pireaux, N. Betz, Polymer 45 (26) (2004) 8683.
[37] Q. Liu, Z. Zhu, X. Yang, X. Chen, Y. Song, Radiat. Phys. Chem. 76 (4) (2007) 707.
[38] G. Zhai, E.T. Kang, K.G. Neoh, Macromolecules 37 (19) (2004) 7240.
[39] Y.W. Kim, D.K. Lee, K.J. Lee, J.H. Kim, Eur. Polym. J. 44 (3) (2008) 932.
[40] H. Bouhamed, S. Boufi, A. Magnin, J. Colloid Interface Sci. 261 (2) (2003) 264.
[41] T. Miyazawa, T. Shimanouchi, S. Mizushima, J. Chem. Phys. 24 (2) (1956) 408.
[42] P. Adhikary, S. Krishnamoorthi, J. Appl. Polym. Sci. 126 (S1) (2012) E313.
[43] X. Shen, X. Yin, Y. Zhao, L. Chen, Colloid Polym. Sci. 293 (4) (2015) 1205.
[44] A. Salimi, A.A. Yousefi, Polym. Test. 22 (6) (2003) 699.
[45] R. Gregorio, E.M. Ueno, J. Mater. Sci. 34 (18) (1999) 4489.
[46] M. Benz, W.B. Euler, J. Appl. Polym. Sci. 89 (4) (2003) 1093.
[47] G.T. Davis, J.E. McKinney, M.G. Broadhurst, S.C. Roth, J. Appl. Phys. 49 (10) (1978) 4998.
[48] A. Manuel Stephan, Eur. Polym. J. 42 (1) (2006) 21.
[49] D.T. Hallinan, N.P. Balsara, Annu. Rev. Mater. Res. 43 (1) (2013) 503.
[50] A.S. Shaplov, R. Marcilla, D. Mecerreyes, Electrochim. Acta 175 (2015) 18.